Quantum coherence of bulk electrons on metals revealed by scanning tunneling spectroscopy

Robin Ohmann,[1,2] Cormac Toher,[1,*] Jörg Meyer,[1,2] Anja Nickel,[1,2] Francesca Moresco,[1,2,†] and Gianaurelio Cuniberti[1,2]
[1]*Institute for Materials Science and Max Bergmann Center of Biomaterials, TU Dresden, 01062 Dresden, Germany*
[2]*Center for Advancing Electronics Dresden, TU Dresden, 01062 Dresden, Germany*
(Received 23 January 2014; revised manuscript received 7 May 2014; published 27 May 2014)

The quantum dynamics of electrons in bulk states is investigated by scanning tunneling microscopy and spectroscopy on a Ag(100) surface. By measuring conductance maps above a threshold voltage, we observe standing waves at step edges and defects. We interpret these to originate from electrons in a bulk band edge at the Γ point. From the spatially decaying waves, the wave vector and the quantum coherence parameters—coherence length, lifetime, and linewidth—are determined as a function of energy. We measure a coherence length of about 5–7 Å, which is order of magnitudes lower than typically observed for surface or image-potential states. The energy of the band edge is extracted from the dispersion relation and agrees with the peak measured in scanning tunneling spectra at 1.9 eV above the Fermi energy. Theoretical calculations confirm the nature of the state elucidating the experimental findings.

DOI: 10.1103/PhysRevB.89.205433 PACS number(s): 71.20.Be, 68.37.Ef, 71.15.Mb

I. INTRODUCTION

The dynamics of electrons in materials plays a fundamental role for electron transport and electronic excitations as well as for adsorbate interactions which are mediated by the electronic states of the substrate. Even though scanning tunneling microscopy (STM) is foremost a surface sensitive technique, it has been shown that electronic properties of the bulk are also detectable as they can extend onto the surface. For example, the scattering of electrons at subsurface impurities leads to charge density oscillations on the surface offering information about the bulk [1,2]. Electrons scattered at step edges and adsorbates also cause scattering patterns, in the form of standing waves on the surface. These standing waves typically originate from surface states [3–5] or image-potential states [6]. However, the bulk states are also held responsible for some of the observed standing waves on selected metal surfaces [7–9]. From the observed quantum interference patterns the electron dynamics can be extracted. So far, only electrons confined in two dimensions, as present in surface states or image-potential states, have been measured by scanning tunneling spectroscopy with respect to their quantum coherence [6,10]. Since the scattering properties are expected to change with the dimensionality of the electron gas [11], it is *a priori* not clear how the scattering of bulk state electrons will occur as they are free to propagate in three dimensions. Whereas the dispersion relation of electrons in bulk states has been measured by Fourier-transform scanning tunneling microscopy [7–9], that is, extracting the wave vector from dI/dV images of the surface, this technique does not provide any quantitative information about the quantum coherence.

In this paper, we investigate the quantum coherence of bulk state electrons with scanning tunneling spectroscopy. By measuring and analyzing the conductance perpendicular to a step edge of a metal surface we obtain, in addition to the dispersion relation, information about the coherence length, the lifetime, and the linewidth. As a model system we use Ag(100) as no surface state is reported at the Γ point providing direct access to the bulk states. The use of STM offers the advantage that local effects can also be investigated, allowing for the separate observation of scatterers with different dimensions, such as step edges or atomic defects. Calculations using density functional theory (DFT) were performed to elucidate the experimental observations.

II. RESULTS AND DISCUSSION

The Ag(100) single crystal was prepared by standard annealing and sputtering cycles and then transferred into the STM, where it was cooled down to 5 K. Step edges were created by dipping the tip of the STM into the surface, resulting in clean and straight edges. In Fig. 1(a) (top) a topography

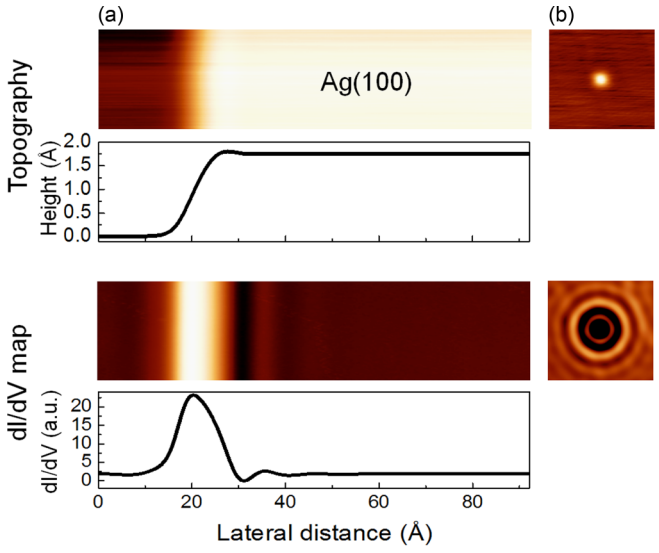

FIG. 1. (Color online) (a) Topography and simultaneously acquired differential conductance dI/dV map of an artificially created step edge on Ag(100). The graphs show the respective averaged line scans. (b) Topography and conductance map of a defect on Ag(100). Image parameters: (a) Bias = 2.7 V, image size 92.2 Å^2 × 21.1 Å^2; (b) 0.1 V (top), 3.0 V (bottom), 52 Å^2 × 49 Å^2.

*Present address: Department of Mechanical Engineering and Materials Science, Duke University, Durham, NC 27708, USA.
†francesca.moresco@nano.tu-dresden.de

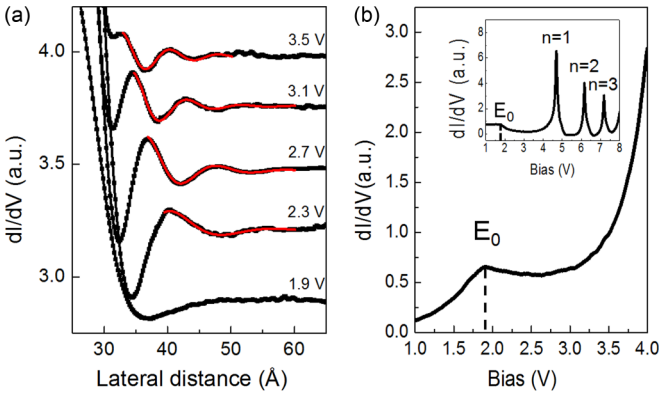

FIG. 2. (Color online) (a) Conductance measured perpendicular to a step edge of Ag(100) at selected energies. Squares represent experimental data points and red lines denote the corresponding fit. Current = 1 nA. Lock-in parameters: Modulation amplitude 20 mV and time constant 100 ms. Average over ten lines. (b) STS spectra measured on the bare Ag(100) surface. Inset shows an extended voltage range up to the image-potential states. All spectra are taken with the feedback loop closed.

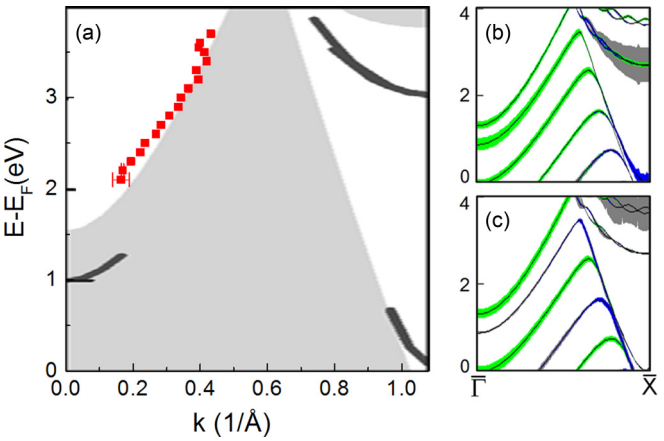

FIG. 3. (Color online) (a) Dispersion relation: Experimental data points (red squares). For clarity error bars smaller than the squares have been omitted. In the background theoretical calculations of the projected bulk band structure are displayed (taken from Ref. [22]). (b), (c) Calculated band structure with the projection on (b) the surface layer and (c) the central layer. The colors represent the projection on the specific orbitals. The projection on the s orbitals is highlighted in gray, the projections on the p_x and p_y orbitals (i.e., parallel to the plane of the surface) are highlighted in blue and red, and the projection on the p_z orbitals (perpendicular to the plane of the surface) is highlighted in green.

image of such a step edge is shown. A simultaneously acquired differential conductance map of the same area is displayed in Fig. 1(a) (bottom). In the conductance image as well as in the line scan, one can clearly see periodic modulations, indicating standing wave patterns. These patterns have also been observed at defects such as shown in Fig. 1(b) and are characteristic for a nearly free electron gas.

In order to measure the dispersion relation, dI/dV maps of the step edge were acquired at different energies. Line scans were extracted running perpendicular to the step edge [see Fig. 2(a) for selected energies]. These line scans were fitted by the following function [14], which applies to spatially decaying quantum interference patterns at step edges:

$$\mathrm{LDOS}(E,x) = L_0\{1-re^{-(x-x_0)/L_\Phi}J_0[2k_p(x-x_0)]\} + \mathrm{offset}. \quad (1)$$

Here, x_0 is the position of the step edge, x is the lateral position, k_p is the wave vector parallel to the surface, L_Φ is the phase coherence length, L_0 is a proportionality constant, r is the reflectivity of the step edge, and J_0 is the Bessel function of zeroth order. The equation is valid for $x > \pi/k$ [10]. Fits for selected energies are shown in Fig. 2(a). The physically relevant parameters are the wave vector k_p and the phase coherence length L_Φ, which both depend on the energy E of the incident electron being determined by the applied bias voltage. The extracted dispersion relation, that is, the energy E as a function of the wave vector k_p, is shown in Fig. 3(a). A parabola can be fitted, with

$$E = \frac{\hbar^2 k_p^2}{2m^*} + E_0, \quad (2)$$

where $\hbar$ is the reduced Planck constant and the fitting parameters are the energy onset E_0 and the effective mass m^*. The fit yields $E_0 = 1.9(1)$ eV for the energy onset and $m^* = 0.41(2)m_e$ for the effective mass. The positive energy value means that it is an unoccupied state. Indeed, when taking scanning tunneling spectra (STS) on the bare Ag(100) surface we do see a feature at 1.9 V [see Fig. 2(b)], which can be interpreted as the onset of the band gap [15]. This peak is observed even far away from the step edge, in contrast to electronic localization phenomena only found on top or in close proximity of adsorbates [16] and step edges [17]. For larger voltages, no additional feature can be seen until the first image-potential state at about 4.7 V [see inset Fig. 2(b)] [18].

In order to understand the nature of the observed electronic state, DFT calculations were carried out for a silver slab with a thickness of 11 atomic layers. The calculations were performed using the *ab initio* program VASP (Vienna *ab initio* simulation program) [19,20]. This method allows for the specification of the orbital character of the calculated electronic bands. The local density approximation exchange-correlation functional and projector augmented-wave methods [20,21] were used, and a value of 250 eV was used for the energy cutoff for the plane-wave basis set. The calculated band structures are shown in Figs. 3(b) and 3(c). The calculated band structure is similar to those previously described in the literature [22,23]. In particular, there are several band minima at the Γ point in the energy range from E_F to $E_F + 1.5$ eV. Here, we can also assign the orbital character. As can be seen in Figs. 3(b) and 3(c), the bands with the minima at the Γ point in the energy range from E_F to $E_F + 1.5$ eV are primarily due to p orbitals (highlighted in green) oriented perpendicular to the plane of the surface. The p orbitals extend much further into the vacuum and thus are more accessible to the scanning tunneling microscope. To elucidate the location of the state in the crystal, the projections of the bands are shown for the surface layer [Fig. 3(b)] and for the central layer of the slab [Fig. 3(c)]. It can be seen that the weight of the state at the band edge does not reduce

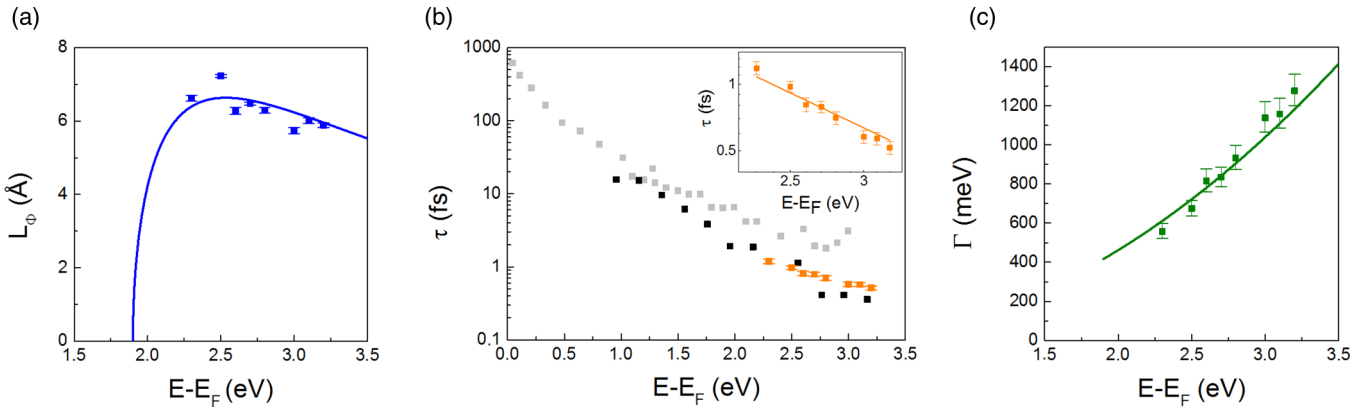

FIG. 4. (Color online) (a) Coherence length, (b) lifetime, and (c) linewidth vs energy. Colored squares represent the experimental data points and the lines are corresponding fits and calculations. The inset in (b) shows the same data in double logarithmic scale. In (b) the lifetime is compared to bulk values of Ag as obtained with the time-resolved two-photon photoemission (TR-2PPE) technique [12,13] (black and gray squares, respectively).

when going into the bulk. A reduction would be expected for a surface state, as can be seen clearly for the known surface state at the X point at 3 eV. As the contribution of the state at the band edge in the bulk is still substantial, we therefore assign the observed standing waves to the bulk states. This conclusion is in agreement with the absence of a surface state in this region of the band structure in both the experimental and theoretical literature. Calculations along other in-plane crystal directions reveal that the band edge is rotationally symmetric around the Γ point in accordance with the experimental result of standing waves around a defect, which have rotational symmetry [see Fig. 1(b)].

Having established the nature of the electronic feature to be assigned to the bulk properties, we now turn to a more detailed investigation of the electron dynamics. From the fits of the conductance close to a step edge, the coherence length L_Φ can also be extracted. The coherence length or phase-relaxation length is the average distance that an electron travels before it experiences inelastic scattering destroying its initial coherent state. The measured coherence length is shown in Fig. 4(a) as a function of energy. It can be seen that for all acquired energies the coherence length is rather short, in the order of 5–7 Å. This length is much lower than observed for other standing wave patterns, such as typically obtained for image potential states [i.e., 40 Å on Cu(100) [6]] or surface states measured close to the Fermi energy, where the coherence length can theoretically even become infinitely large. Experimental values of more than 300 Å have been reported in [24]. To further elucidate the dynamics of the electrons, we look at their lifetime. The lifetime τ can be calculated from the coherence length via

$$\tau = \frac{L_\Phi}{v} = \frac{L_\Phi m^*}{\hbar k_p}, \tag{3}$$

where v is the group velocity. This conversion is possible as the coherence length is smaller than the local elastic mean free path of the electrons [25]. The latter is confirmed by choosing a sufficiently large defect-free area for the measurements [see Fig. 1(a)]. The lifetime is plotted as a function of energy in Fig. 4(b). The values of the lifetime are in the order of 1 fs or lower. Comparing the lifetime with TR-2PPE measurements on bulk Ag [see Fig. 4(b)], we find good agreement. Using Fermi-liquid theory the lifetime is fitted via the following expression:

$$\tau = \lambda(E - E_F)^{-2}, \tag{4}$$

where E_F is the Fermi energy and λ is the fitting parameter [26]. For λ we obtain a value of 5.7(2) fs eV^2. This is comparable to that on Ag(111) [10]. For other metal surfaces different prefactors were reported. This suggests that the lifetime does not depend on the orientation of the surface, but only on the type of metal. Additionally, the linewidth has been determined via the following relation:

$$\Gamma = \frac{\hbar}{\tau} \tag{5}$$

and is plotted in Fig. 4(c). Using Eqs. (2)–(4) the coherence length can be described by

$$L_\Phi = \lambda(E - E_F)^{-2}\frac{\hbar k_p}{m^*} = \frac{\lambda\sqrt{2}}{\sqrt{m^*}}\frac{\sqrt{E - E_0}}{(E - E_F)^2} \tag{6}$$

as plotted in Fig. 4(a) (full line). Interestingly, for partially occupied surface states, that is, for states which cross the Fermi level, a singularity in the coherence length is present. However, as the onset energy on Ag(100) is above the Fermi level, no such singularity exists. Additionally, the coherence length gets smaller with increasing energy. In the present case the lowest energy is 1.9 eV, which is already very large. We attribute the observed small coherence length to the fact that the energetic onset is far above the Fermi energy. The maximum of the coherence length for states crossing the Fermi level is always at the Fermi level. The question which arises is, at which energy does the coherence length have its maximum for unoccupied states? Differentiating the equation for the coherence length given in (6) and setting it to zero, one finds for the energies with respect to the Fermi level at which the maximum of the coherence length is obtained the very simple expression

$$E_{L_\Phi(\max)} = \tfrac{4}{3}E_0. \tag{7}$$

Importantly, such a result is very general as the energy where the coherence length has its maximum is solely determined by the energy onset (E_0) and no other parameter. The other material constants cancel out when the derivative is set to zero.

The maximum is obtained by the competition of the numerator and denominator in the fraction given in Eq. (6). The prefactor 4/3 in (7) is determined by the ratio of the exponents in (6) (exponent of denominator divided by difference of exponent of denominator and numerator) and thus can be attributed to a constant which is determined by the nature of the system. In the case here, it is the nearly free electron gas.

Lastly, we discuss the decay rate, that is, how fast the amplitude decreases as a function of distance from the scatterer. The decay of the intensity is described by

$$\propto \frac{1}{(x - x_0)^a}, \tag{8}$$

where x is the lateral position, x_0 is the position of the scatterer, and a is the decay parameter [7,11]. For the step edge we obtain a value of 3.0(8) and for the point scatterer 1.8(5) for the decay parameter. The relatively large error is attributed to the width of the step edge (±5 Å) and to the low number of maxima which are available for the fitting. Nevertheless, a trend to a higher decay rate than observed in image-potential and surface states [27], which are confined to two dimensions, becomes apparent for the three-dimensional bulk states. A full theoretical treatment of the decay channels such as electron-electron interactions is currently ongoing.

III. CONCLUSION

In conclusion, we have shown energy dependent quantum interference patterns on the Ag(100) surface measured with scanning tunneling microscopy. These are caused by scattering of electrons within a bulk state reaching out to the surface. The measured dispersion relation is parabolic with an effective mass of $0.41m_e$ and a state onset of 1.9 eV above the Fermi energy. This onset lies at the projected band-gap onset of the Ag(100) surface at the Γ point, as evidenced by DFT calculations. The lifetime, linewidth, and coherence length have been precisely measured as a function of energy gaining insight into the quantum coherence of the bulk bands. In addition, the decay parameter has been determined for scattering at defects and step edges. Our results are important for the understanding of the quantum dynamics of bulk states of metals and are expected to have an impact on electronic excitation and adsorbate interaction phenomena.

ACKNOWLEDGMENTS

This research was funded by the ICT-FET European Union Integrated Project AtMol, the European Union (ERDF), the Free State of Saxony via the ESF Project 100087859 ENano, ECEMP A2, and the Deutsche Forschungsgemeinschaft (DFG) and National Science Foundation (NSF) (NSF 11-568). We gratefully acknowledge support from the German Excellence Initiative via the Cluster of Excellence EXC 1056 "Center for Advancing Electronics Dresden" (cfaed). The authors thank Mario Rocca for fruitful discussions. Computational facilities were provided by Zentrum für Informationsdienste und Hochleistungsrechnen (ZIH) at TU Dresden.

[1] A. Weismann, M. Wenderoth, S. Lounis, P. Zahn, N. Quaas, R. G. Ulbrich, P. H. Dederichs, and S. Blügel, Science **323**, 1190 (2009).
[2] C. Sprodowski and K. Morgenstern, Phys. Rev. B **82**, 165444 (2010).
[3] M. F. Crommie, C. P. Lutz, and D. M. Eigler, Nature (London) **363**, 524 (1993).
[4] Y. Hasegawa and Ph. Avouris, Phys. Rev. Lett. **71**, 1071 (1993).
[5] G. M. Rutter, J. N. Crain, N. P. Guisinger, T. Li, P. N. First, and J. A. Stroscio, Science **317**, 219 (2007).
[6] P. Wahl, M. A. Schneider, L. Diekhöner, R. Vogelgesang, and K. Kern, Phys. Rev. Lett. **91**, 106802 (2003).
[7] L. Petersen, P. Laitenberger, E. Lægsgaard, and F. Besenbacher, Phys. Rev. B **58**, 7361 (1998).
[8] K. Schouteden, P. Lievens, and C. Van Haesendonck, Phys. Rev. B **79**, 195409 (2009).
[9] J. I. Pascual, A. Dick, M. Hansmann, H.-P. Rust, J. Neugebauer, and K. Horn, Phys. Rev. Lett. **96**, 046801 (2006).
[10] L. Bürgi, O. Jeandupeux, H. Brune, and K. Kern, Phys. Rev. Lett. **82**, 4516 (1999).
[11] J. M. Ziman, *Principles of the Theory of Solids* (Cambridge University Press, Cambridge, 1972).
[12] M. Aeschlimann, M. Bauer, and S. Pawlik, Chem. Phys. **205**, 127 (1996).
[13] M. Wolf and M. Aeschlimann, Phys. Bl. **54**, 145 (1998).
[14] S. Crampin, J. Kröger, H. Jensen, and R. Berndt, Phys. Rev. Lett. **95**, 029701 (2005).
[15] A. Goldmann, V. Dose, and G. Borstel, Phys. Rev. B **32**, 1971 (1985).
[16] L. Limot, E. Pehlke, J. Kröger, and R. Berndt, Phys. Rev. Lett. **94**, 036805 (2005).
[17] L. Bartels, S. W. Hla, A. Kühnle, G. Meyer, K.-H. Rieder, and J. R. Manson, Phys. Rev. B **67**, 205416 (2003).
[18] H.-C. Ploigt, C. Brun, M. Pivetta, F. Patthey, and W.-D. Schneider, Phys. Rev. B **76**, 195404 (2007).
[19] G. Kresse and J. Furthmüller, Phys. Rev. B **54**, 11169 (1996).
[20] G. Kresse and D. Joubert, Phys. Rev. B **59**, 1758 (1999).
[21] P. E. Blöchl, Phys. Rev. B **50**, 17953 (1994).
[22] L. Savio, L. Vattuone, M. Rocca, V. De Renzi, S. Gardonio, C. Mariani, U. del Pennino, G. Cipriani, A. Dal Corso, and S. Baroni, Surf. Sci. **486**, 65 (2001).
[23] H. Erschbaumer, A. J. Freeman, C. L. Fu, and R. Podlouckly, Surf. Sci. **243**, 317 (1991).
[24] L. Vitali, P. Wahl, M. A. Schneider, K. Kern, V. M. Silkin, E. V. Chulkov, and P. M. Echenique, Surf. Sci. **523**, L47 (2003).
[25] S. Datta, *Electronic Transport in Mesoscopic Systems* (Cambridge University Press, Cambridge, 1995).
[26] W.-D. Schöne, Prog. Surf. Sci. **82**, 161 (2007).
[27] Ph. Avouris, I. W. Lyo, R. E. Walkup, and Y. Hasegawa, J. Vac. Sci. Technol. B **12**, 1447 (1994).